

Performance of the BGSDC integrator for computing fast ion trajectories in nuclear fusion reactors[☆]

Krasymyr Tretiak^{a,*}, James Buchanan^b, Rob Akers^b, Daniel Ruprecht^c

^a*School of Mathematics, University of Leeds, United Kingdom*

^b*CCFE, Culham Science Centre, Abingdon, United Kingdom*

^c*Lehrstuhl Computational Mathematics, Institut für Mathematik, Technische Universität Hamburg, Germany*

Abstract

Modelling neutral beam injection (NBI) in fusion reactors requires computing the trajectories of large ensembles of particles. Slowing down times of up to one second combined with nanosecond time steps make these simulations computationally very costly. This paper explores the performance of BGSDC, a new numerical time stepping method, for tracking ions generated by NBI in the DIII-D and JET reactors. BGSDC is a high-order generalisation of the Boris method, combining it with spectral deferred corrections and the Generalized Minimal Residual method GMRES. Without collision modelling, where numerical drift can be quantified accurately, we find that BGSDC can deliver higher quality particle distributions than the standard Boris integrator at comparable cost or comparable distributions at lower cost. With collision models, quantifying accuracy is difficult but we show that BGSDC produces stable distributions at larger time steps than Boris.

Keywords: fast ions, Boris integrator, particle tracking, spectral deferred corrections, DIII-D, JET, neutral beam injection

[☆]This work was supported by the Engineering and Physical Sciences Research Council EPSRC under grant EP/P02372X/1 “A new algorithm to track fast ions in fusion reactors”.

*Corresponding author

Email addresses: k.tretiak@leeds.ac.uk (Krasymyr Tretiak),
james.buchanan@ukaea.uk (James Buchanan), Rob.Akers@ukaea.uk (Rob Akers),
ruprecht@tuhh.de (Daniel Ruprecht)

1. Introduction

Computer simulations are a critical tool for the design and operation of fusion reactors [1]. Numerical computation of the trajectories of fast ions generated, for example, from neutral beam injection is important to minimise wall loads and energy loss from ions escaping magnetic confinement [2]. At their core, particle trackers integrate the Lorentz equations

$$\dot{\mathbf{x}}(t) = \mathbf{v}(t) \tag{1a}$$

$$\dot{\mathbf{v}}(t) = \alpha [\mathbf{E}(\mathbf{x}) + \mathbf{v} \times \mathbf{B}(\mathbf{x})] =: \mathbf{f}(\mathbf{x}, \mathbf{v}). \tag{1b}$$

for a large ensemble of particles and use the resulting trajectories to generate statistical quantities like wall load. Note that fast ions in fusion reactors are typically not fast enough to require consideration of relativistic effects and so the non-relativistic Lorentz equations can be used.

Fast ions interact with the plasma and deposit energy, thus heating it. To compute steady-state distributions, trajectories need to be computed until the fast ions lose their energy through collisions and thermalise. This slowing down time over which an ensemble of trajectories needs to be calculated depends on the energy of the ions when injected and the bulk plasma parameters. For DIII-D, the required simulation time is around 0.1 s. For the larger JET, it is around 1 s. Because resolving gyro effects requires time steps of the order of nanoseconds, simulations involve many millions of time step, leading to substantial computational cost and thus long solution times. Simulating a full ensemble of fast ions in JET until thermalisation takes several days, despite making use of modern GPU clusters.

Some models, for example NUBEAM [3, 4] or OFMC [5], use a guiding centre approximation where gyro effects are neglected or only included once a particle is near the walls. This allows to take larger time step and thus reduces computational cost. However, taking orbit effects into consideration is important to generate realistic wall loads [6]. Other particle tracking codes, for example ASCOT [7] and LOCUST [8], compute the full equations with

gyro effects. For numerical methods, the only choices available are the Boris integrator (ASCOT seems to use the Verlet variant whereas LOCUST uses the Leapfrog version) and the Cash-Karp Runge-Kutta 4(5) method [9]. LOCUST also features a mover based on Strang splitting, which is very similar to Boris but avoids some issues around loss of accuracy in cylindrical coordinates [10]. There seems to be agreement that due to its significant energy drift, RK4(5) is less efficient than Boris and so the latter is typically used. Although Boris is surprisingly efficient [11], long solution times remain an issue. While other algorithms have been proposed for solving the Lorentz equations [12, 13, 14, 15, 16, 17], they have so far not been adopted for fast ion tracking.

Tretiak and Ruprecht [18] introduce BGSDC, a new high-order algorithm for solving the Lorentz equations based on a combination of spectral deferred corrections, a Generalized Minimal Residual (GMRES) iteration and the Boris integrator. They show improvements in computational performance over Boris for individual particle trajectories in a mirror trap as well as trapped and passing particles in a Sulev'ev equilibrium.

This paper extends their results by demonstrating performance for realistic test cases, studying practically relevant, aggregate quantities to assess quality of solutions instead of individual trajectories. Instead of analytically given idealized magnetic fields, we use the actual magnetic equilibrium of DIII-D and JET including interpolation. In the non-collisional case, we track particle ensembles corresponding to real neutral beam injection (NBI) scenarios [2, 19] and assess statistical distribution of particle drift in the ensemble in contrast to exploring accuracy of individual trajectories. We show that BGSDC delivers distributions with smaller standard deviation than Boris and, if standard deviations of the order of micrometers are desired, can deliver them with less computational work. Then, we investigate the case where models for collisions of fast ions with the plasma are active. While the stochastic nature of these results makes a quantitative assessment with respect to work versus precision difficult, we demonstrate that BGSDC can deliver similar results as Boris with larger time steps. Delivering additional evidence to show that these gains are

enough to also deliver computational gains in the collisional case will require a more developed framework to quantify accuracy for the generated statistical distributions as well as substantially more computational results and is left for future work. Our results demonstrate that there can be a computational benefit from using BGSDC or other particle trackers with order of accuracy higher than two, in particular for high fidelity simulations with tight accuracy requirements.

All results were generated with the BGSDC implementation [20] that is now part of the LOCUST code and the ITER Integrated Modelling & Analysis Suite (IMAS) [21].

2. Methodology

The GMRES-accelerated Boris-SDC algorithm (or BGSDC for short) is described in detail by Tretiak et al. in 2019 [18] whereas its predecessor, without GMRES-acceleration, was introduced by Winkel et al. [22]. This original Boris-SDC combined the Boris algorithm introduced by Boris in 1970 [23] with spectral deferred corrections (SDC) introduced by Dutt et al. in 2000 [24] to generalize it to higher order. BGSDC incorporates a GMRES-based convergence accelerator for SDC, introduced by Huang et al. in 2006 [25] for first order problems, that leads to improved long-term energy stability. All simulation results reported in this paper were generated using a BGSDC implementation in the GPU-accelerated LOCUST particle tracking code developed at CCFE.

2.1. Collocation Methods

In essence, BGSDC is an iterative solver for a collocation method. Over one time step $[t_n, t_{n+1}]$, the Lorentz equations (1) written in integral form become

$$\mathbf{x}(t) = \mathbf{x}_0 + \int_{t_n}^t \mathbf{v}(s) ds \quad (2a)$$

$$\mathbf{v}(t) = \mathbf{v}_0 + \int_{t_n}^t \mathbf{f}(\mathbf{x}(s), \mathbf{v}(s)) ds \quad (2b)$$

with \mathbf{x}_0 , \mathbf{v}_0 being approximations of position and velocity at time t_n brought forward from the previous step. Note that we consider only the case where

the electric and magnetic field vary in space but not in time, but the method can easily be generalised to the non-autonomous case. Typically, Boris method is based on a Leapfrog discretization of the differential form of the Lorentz equations (1). Here, we use a variant based on the Velocity-Verlet method instead

$$\mathbf{x}_{n+1} = \mathbf{x}_n + \Delta t \left(\mathbf{v}_n + \frac{\Delta t}{2} \mathbf{f}(\mathbf{x}_n, \mathbf{v}_n) \right) \quad (3a)$$

$$\mathbf{v}_{n+1} = \mathbf{v}_n + \frac{\Delta t}{2} (\mathbf{f}(\mathbf{x}_n, \mathbf{v}_n) + \mathbf{f}(\mathbf{x}_{n+1}, \mathbf{v}_{n+1})), \quad (3b)$$

see Tretiak et al. for a discussion [18]. A geometric trick was introduced by Boris in 1970 [23] to avoid the seemingly implicit dependence on \mathbf{v}_{n+1} . Birdsall and Langdon give a detailed description [26, Section 4-4].

Collocation methods discretise the integral form (2) using numerical quadrature with nodes $t_n \leq \tau_1 < \dots < \tau_M \leq t_{n+1}$ instead of the differential form. Approximate values \mathbf{x}_{new} and \mathbf{v}_{new} at time t_{n+1} are computed via

$$\mathbf{x}_{\text{new}} = \mathbf{x}_0 + \sum_{m=1}^M q_m \mathbf{v}_m \quad (4a)$$

$$\mathbf{v}_{\text{new}} = \mathbf{v}_0 + \sum_{m=1}^M q_m \mathbf{f}(\mathbf{x}_m, \mathbf{v}_m) \quad (4b)$$

where q_m are quadrature weights while $\mathbf{x}_m, \mathbf{v}_m$ are approximations to position and velocity at the quadrature nodes τ_m . These are equivalent to the stages of a collocation method, an implicit Runge-Kutta method with a dense Butcher tableau [27, Theorem 7.7], and can be computed or approximated by solving the stage equations

$$\mathbf{x}_m = \mathbf{x}_0 + \sum_{j=1}^M q_{m,j} \mathbf{v}_j \quad (5a)$$

$$\mathbf{v}_m = \mathbf{v}_0 + \sum_{j=1}^M q_{m,j} \mathbf{f}(\mathbf{x}_j, \mathbf{v}_j). \quad (5b)$$

Depending on the choice of quadrature nodes, collocation methods can have a range of desirable properties. They are symplectic for Gauss-Legendre nodes [27, Theorem 16.5] and symmetric for Gauss-Lobatto nodes [28, Theorem 8.9] as well

as A-stable [29, Theorem 12.9]. By combining the stages $\mathbf{x}_m, \mathbf{v}_m$ into one vector \mathbf{U} , the stage equations (5) can compactly be written as a nonlinear system

$$\mathbf{U} - \mathbf{Q}\mathbf{F}(\mathbf{U}) = \mathbf{U}_0 \quad (6)$$

with \mathbf{Q} containing quadrature weights,

$$\mathbf{F}(\mathbf{U}) = (\mathbf{v}_1, \dots, \mathbf{v}_M, \mathbf{f}(\mathbf{x}_1, \mathbf{v}_1), \dots, \mathbf{f}(\mathbf{x}_M, \mathbf{v}_M)), \quad (7)$$

and \mathbf{U}_0 containing repeated entries of \mathbf{x}_0 and \mathbf{v}_0 . See Winkel et al. for details [22].

2.2. Boris-GMRES-SDC (BGSDC)

Spectral deferred corrections use an iteration based on a low order method to solve Eq. (6). For first order problems, this is typically an implicit or implicit-explicit Euler [24, 30]. For second order problems, velocity-Verlet integration or, in the special case of the Lorentz equations, the Boris integrator can be used [22]. If the collocation problem (6) is linear and thus, in a slight abuse of notation, reads

$$(\mathbf{I} - \mathbf{Q}\mathbf{F})\mathbf{U} = \mathbf{U}_0, \quad (8)$$

one can apply a preconditioned GMRES iteration instead of SDC to solve it [25]. The key point is that GMRES does not require assembly of the system matrix but only a function that applies $\mathbf{I} - \mathbf{Q}\mathbf{F}$ to a given vector \mathbf{U} . This simply means computing Eq. (5) for $m = 1, \dots, M$. However, to improve performance, it is advisable to use a preconditioner. In the GMRES interpretation, the low order base method (Euler in the first order case, Boris in the second order case) can be understood as a preconditioner, modifying the original collocation system (6) to

$$(\mathbf{I} - \mathbf{Q}_{\Delta t}\mathbf{F})^{-1}(\mathbf{I} - \mathbf{Q}\mathbf{F})\mathbf{U} = (\mathbf{I} - \mathbf{Q}_{\Delta t}\mathbf{F})^{-1}\mathbf{U}_0, \quad (9)$$

where $\mathbf{Q}_{\Delta t}$ has a block structure with each block being a lower triangular matrix [18]. To apply GMRES to the preconditioned problem, a second function is required that can solve

$$(\mathbf{I} - \mathbf{Q}_{\Delta t}\mathbf{F})\mathbf{U} = \mathbf{b} \quad (10)$$

for a given right-hand side \mathbf{b} [31]. Because of the special structure of \mathbf{Q}_Δ , this can be done in a sweep-like fashion, very similar to the sweeps in the original variant of SDC. When using $M = 3$ nodes, solving Eq. (10) amounts to a block-wise solve of

$$\begin{bmatrix} \mathbf{x}_1 \\ \mathbf{x}_2 \\ \mathbf{x}_3 \end{bmatrix} - \begin{bmatrix} 0 & 0 & 0 \\ \Delta\tau_2\mathbf{I} & 0 & 0 \\ \Delta\tau_2\mathbf{I} & \Delta\tau_3\mathbf{I} & 0 \end{bmatrix} \begin{bmatrix} \mathbf{v}_1 \\ \mathbf{v}_2 \\ \mathbf{v}_3 \end{bmatrix} - \frac{1}{2} \begin{bmatrix} 0 & 0 & 0 \\ \Delta\tau_2^2\mathbf{I} & 0 & 0 \\ \Delta\tau_2^2\mathbf{I} & \Delta\tau_3^2\mathbf{I} & 0 \end{bmatrix} \begin{bmatrix} \mathbf{F}(\mathbf{x}_1, \mathbf{v}_1) \\ \mathbf{F}(\mathbf{x}_2, \mathbf{v}_2) \\ \mathbf{F}(\mathbf{x}_3, \mathbf{v}_3) \end{bmatrix} = \begin{bmatrix} \mathbf{b}_1 \\ \mathbf{b}_2 \\ \mathbf{b}_3 \end{bmatrix}$$

and

$$\begin{bmatrix} \mathbf{v}_1 \\ \mathbf{v}_2 \\ \mathbf{v}_3 \end{bmatrix} - \frac{1}{2} \begin{bmatrix} \Delta\tau_1\mathbf{I} & 0 & 0 \\ (\Delta\tau_1 + \Delta\tau_2)\mathbf{I} & \Delta\tau_2\mathbf{I} & 0 \\ (\Delta\tau_1 + \Delta\tau_2)\mathbf{I} & (\Delta\tau_2 + \Delta\tau_3)\mathbf{I} & \Delta\tau_3\mathbf{I} \end{bmatrix} \begin{bmatrix} \mathbf{F}(\mathbf{x}_1, \mathbf{v}_1) \\ \mathbf{F}(\mathbf{x}_2, \mathbf{v}_2) \\ \mathbf{F}(\mathbf{x}_3, \mathbf{v}_3) \end{bmatrix} = \begin{bmatrix} \mathbf{b}_4 \\ \mathbf{b}_5 \\ \mathbf{b}_6 \end{bmatrix}$$

via first computing

$$\mathbf{x}_1 = \mathbf{b}_1 \tag{11a}$$

$$\mathbf{v}_1 = \mathbf{b}_4 + \frac{1}{2}\Delta\tau_1\mathbf{F}(\mathbf{x}_1, \mathbf{v}_1), \tag{11b}$$

then

$$\mathbf{x}_2 = \mathbf{b}_2 + \Delta\tau_2\mathbf{v}_1 + \frac{1}{2}\Delta\tau_2^2\mathbf{F}(\mathbf{x}_1, \mathbf{v}_1) \tag{12a}$$

$$\mathbf{v}_2 = \mathbf{b}_5 + \frac{1}{2}(\Delta\tau_1 + \Delta\tau_2)\mathbf{F}(\mathbf{x}_1, \mathbf{v}_1) + \frac{1}{2}\Delta\tau_2\mathbf{F}(\mathbf{x}_2, \mathbf{v}_2), \tag{12b}$$

and finally

$$\mathbf{x}_3 = \mathbf{b}_3 + \Delta\tau_2\mathbf{v}_1 + \Delta\tau_3\mathbf{v}_2 + \frac{1}{2}\Delta\tau_2^2\mathbf{F}(\mathbf{x}_1, \mathbf{v}_1) + \frac{1}{2}\Delta\tau_3^2\mathbf{F}(\mathbf{x}_2, \mathbf{v}_2) \tag{13a}$$

$$\mathbf{v}_3 = \mathbf{b}_6 + \frac{1}{2}(\Delta\tau_1 + \Delta\tau_2)\mathbf{F}(\mathbf{x}_1, \mathbf{v}_1) + \frac{1}{2}(\Delta\tau_2 + \Delta\tau_3)\mathbf{F}(\mathbf{x}_2, \mathbf{v}_2) + \frac{1}{2}\Delta\tau_3\mathbf{F}(\mathbf{x}_3, \mathbf{v}_3) \tag{13b}$$

using Boris' trick to compute the velocities [18]. Note that for a single particle, where $\mathbf{F} = \mathbf{f}$, with given initial values $\mathbf{x}_n, \mathbf{v}_n$ at the beginning of the time step, setting $\mathbf{b}_1 := \mathbf{x}_n + \Delta\tau_1(\mathbf{v}_n + \frac{\Delta\tau_1}{2}\mathbf{F}(\mathbf{x}_n, \mathbf{v}_n))$ and $\mathbf{b}_4 := \mathbf{v}_n + \frac{\Delta\tau_1}{2}\mathbf{F}(\mathbf{x}_n, \mathbf{v}_n)$ means that (11) becomes identical to (3) with $\Delta t = \Delta\tau_1$. For specific choices of $\mathbf{b}_2, \mathbf{b}_3, \mathbf{b}_5$ and \mathbf{b}_6 , the steps (11), (12) and (13) correspond to a total of

three Boris steps (3) with step sizes $\Delta\tau_1$, $\Delta\tau_2$ and $\Delta\tau_3$. However, to apply the GMRES procedure, the algorithm is modified to accept any input for \mathbf{b} . This procedure is straightforward to generalize for any number of nodes M .

For nonlinear collocation problems, it is possible to apply a Newton iteration and use GMRES-SDC to solve the linear inner problems. For the case where the nonlinearity is due to the magnetic field depending on \mathbf{x} , this was found not to be competitive [18]. Instead, we linearize the collocation problem by freezing the magnetic field after the first sweep provides values \mathbf{x}_m^0 for $m = 1, \dots, M$ by approximating

$$\mathbf{F}(\mathbf{U}) \approx \mathbf{F}_{\text{lin}}(\mathbf{X}^0)(\mathbf{U}) =: \begin{pmatrix} \mathbf{v}_1 \\ \vdots \\ \mathbf{v}_M \\ \mathbf{f}(\mathbf{x}_1^0, \mathbf{v}_1) \\ \vdots \\ \mathbf{f}(\mathbf{x}_M^0, \mathbf{v}_M) \end{pmatrix},$$

that is, the electric and magnetic field are evaluated at the approximate position \mathbf{x}_m^0 from the first sweep instead of using the positions \mathbf{x}_m in the argument \mathbf{U} . The linearized system is preconditioned using $(\mathbf{I} - \mathbf{Q}_\Delta \mathbf{F}_{\text{lin}})$ and solved with GMRES. The result is then corrected to account for the nonlinearity by a small number of computationally cheap discrete Picard iterations

$$\mathbf{U}^{k+1} = \mathbf{U}_0 + \mathbf{Q}\mathbf{F}(\mathbf{U}^k). \quad (14)$$

If the fields only changes weakly over a single time step, the solution of the linearized collocation problem will be very close to the nonlinear solution and the Picard iteration converges quickly in very few iterations. BGSDC(k, l) refers to this combination of k GMRES-SDC iterations for the linearized collocation problem followed by l Picard iterations for the fully nonlinear collocation problem.

2.3. *LOCUST-GPU implementation*

LOCUST stands for "Lorentz Orbit Code for Use in Stellarators and Tokamaks" [8, 32]. It is a software platform for solving efficiently the Lorentz equations of motion in the presence of a collision operator that models small angle Coulomb scattering. Kernels are instantiated upon Nvidia GPU hardware as PGI CUDA Fortran kernels which allows millions of Monte Carlo markers to be tracked in a typical simulation. LOCUST is being used extensively to design plasma facing components, e.g. for MAST-U [33], and for studying the physics of fast ion distribution and loss due to Neoclassical Tearing Modes and the application of ELM Control Coils for ITER. It is part of the EUROfusion HALO programme, where it is used to study the implications of finite gyro-radius effects, e.g. for Toroidal Alfvén Eigenmode (TAE) activity in Tokamak plasma [34].

3. Numerical Results

We compare BGSDC against the Leapfrog-based staggered Boris method for tracking fast ions generated by NBI in both the DIII-D and Joint European Torus (JET) tokamak. For both reactors, we study the deterministic case without models for the collision of fast ions with the plasma and the stochastic case with collision models. In the collisionless case, we launch a particle ensemble corresponding to a NBI shot and use the standard deviation of the numerical drift distribution as well as conservation of magnetic moment to compare the quality of both integrators. In the presence of collisions with the plasma, stochasticity makes particle drift measurements of trajectories meaningless and a very large number of markers would be required to get statistically converged results. Therefore, to focus on the impact of the numerical error and minimise the spread of ensembles, we instead study many trajectory realizations for the same particle with identical initial conditions and analyse the effect that time step size has on the resulting distribution function profiles.

3.1. Results for the DIII-D tokamak: non-collisional case

We compare Boris and BGSDC for full orbit simulations in a 2D equilibrium for DIII-D shot #157418. This setup has been used, for example, in fast ion transport studies for applied 3D magnetic perturbations in DIII-D [35]. The fast particle birth list contains 10 000 unique particles derived from an NBI source that is injected counter to the plasma current. The duration of all runs is 100 ms and, for simplicity, we do not include plasma facing components (PFC) in our simulations.

Numerical drift. Fig. 1 shows the distribution of numerical drift for four integrators available in LOCUST at final time $t_{end} = 100$ ms for a particle ensemble in the non-collisional case. All integrators use a fixed time step of $\Delta t = 1$ ns

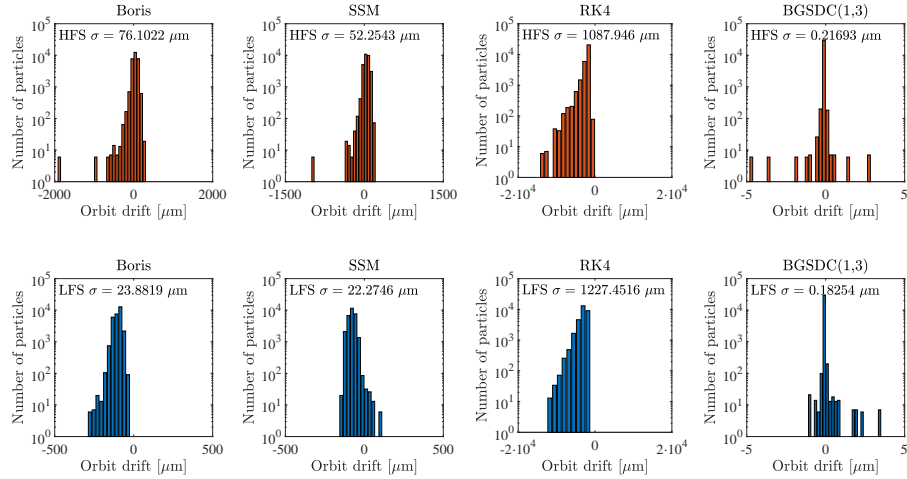


Figure 1: Accuracy comparison of classical Boris, Strang Splitting Mover, Runge-Kutta Cash & Karp and BGSDC(1,3) methods with fixed time step $\Delta t = 1$ ns and $t_{end} = 100$ ms. Please note that the x-axes are scaled differently.

and the same initial conditions for particles. The High Field Side (HFS) drift distributions are shown in the upper two graphs and σ indicates the standard deviation. The lower graphs show the Low Field Side (LFS) drift distributions. The Strang splitting mover and classical Boris deliver comparable accuracy at both sides of the plasma volume. However, the Strang splitting mover requires

more computational work than Boris. RK4 shows unsatisfactory result with very large σ , most likely due to its inherent energy drift. BGSDC(1,3) is more accurate than Boris and Strang, and for both LFS and HFS delivers a σ two orders of magnitude smaller. Of course, it also requires substantially more computational work per time step. Below we will demonstrate that this additional work per time step can be offset by using larger time step sizes and thus computing fewer steps, leading to computational gains when values of σ of around $1\ \mu\text{m}$ or below are required.

Fig. 2 shows the resulting numerical orbital drift of each particle against the major radius R at the end of simulation at $t_{end} = 100\ \text{ms}$. The left fig-

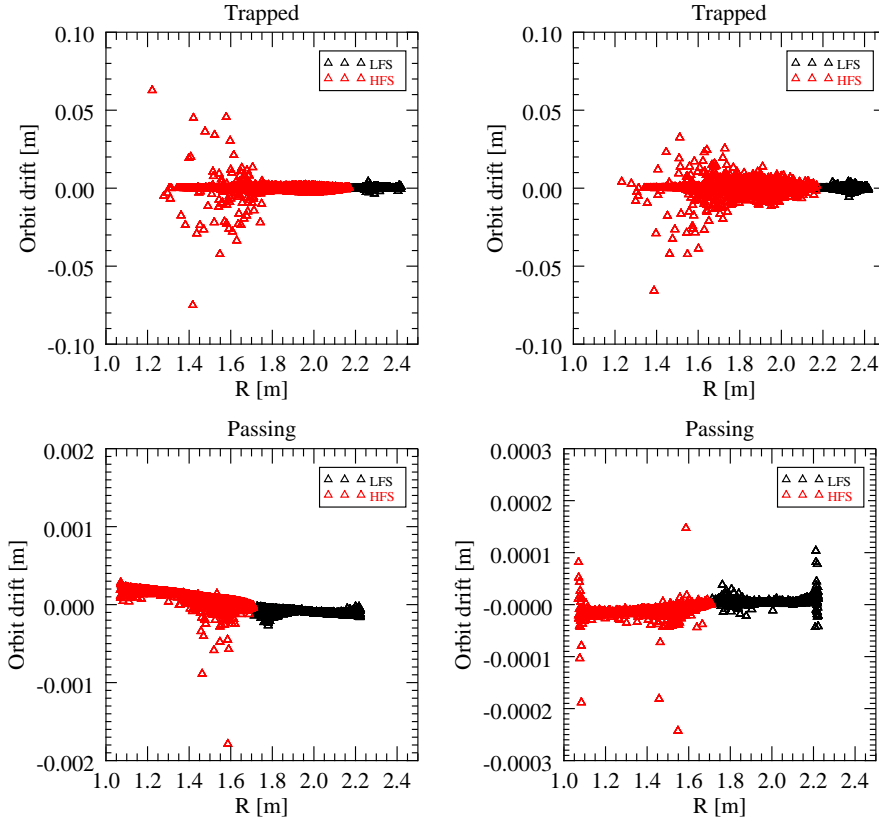


Figure 2: Particle drifts for DIII-D for Boris method with $\Delta t = 1\ \text{ns}$ (left) and BGSDC(2,6) with $\Delta t = 5\ \text{ns}$ (right).

ure is for Boris method with time step 1 ns while the right shows results from BGSDC(2,6) with a time step of 5 ns. The upper graphs show trapped particles, the lower graphs passing particles where particles at the LFS are indicated by black markers and particles at HFS are marked in red. Note that the y -axes in the two lower graphs are scaled differently. For trapped particles, Boris and BGSDC deliver comparable results with particle drifts of up to 5 cm. For passing particles, BGSDC drifts are about an order of magnitude smaller than Boris, despite a five times larger time step.

Fig. 3 shows the frequency distribution of orbital drift in μm for all particles (both trapped and passing) shown in Fig. 2. The upper figures show values at

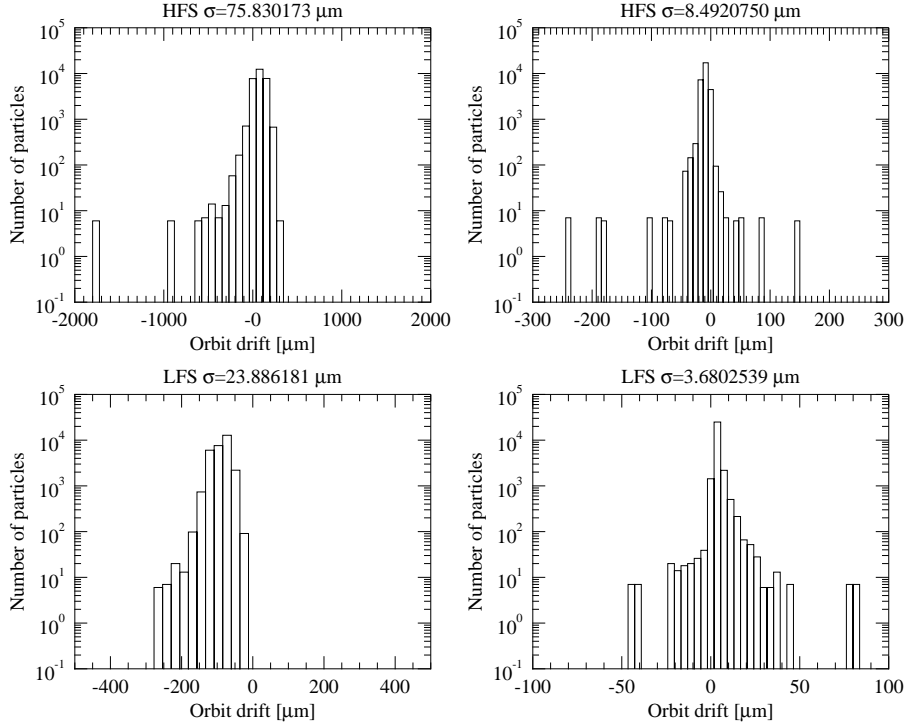


Figure 3: Drift distribution: Boris method $\Delta t = 1 \text{ ns}$ (left) and BGSDC(2,6) $\Delta t = 5 \text{ ns}$ (right).

the HFS, the lower figures at the LFS. The σ in each figure's title indicates the standard deviation for the particle cloud. The smaller σ is, the narrower and thus better is the distribution. At HFS, the standard deviation for BGSDC(2,6)

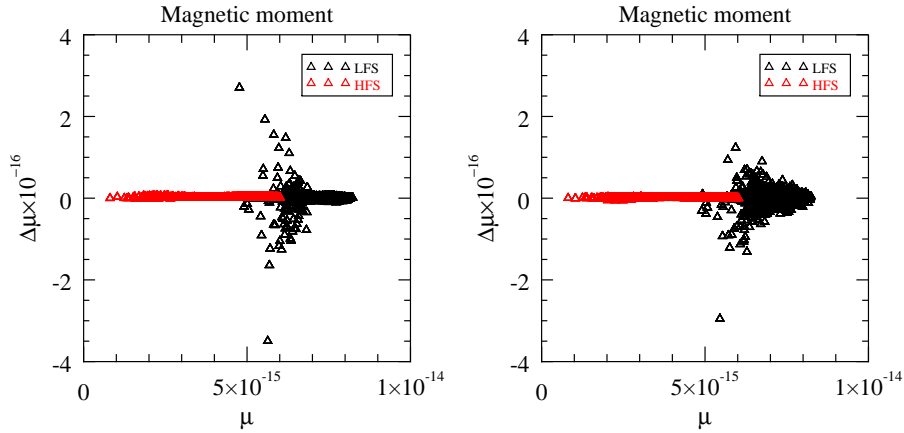


Figure 4: Magnetic moment for Boris method with $\Delta t = 1$ ns (left) and BGSDC(2,6) $\Delta t = 5$ ns (right)

is about nine times smaller than for Boris while at LFS it is a factor of around six more accurate. Furthermore, at LFS, the Boris method seems to have a systematic bias towards negative drift that is not seen in BGSDC.

Magnetic moment. Fig. 4 shows the magnetic moment for all particles along the major radius. Results for the Boris method are shown on the left and for BGSDC(2,6) on the right. Both methods conserve magnetic moment to a very high degree, with errors across all particles being of the order of 10^{-16} .

Accuracy versus time step size. Fig. 5 shows how the standard deviation σ for the HFS (left) and LFS (right) changes with time step size. The higher order of accuracy of both BGSDC(1,3) and BGSDC(2,6) translates into a faster drop of σ with Δt and thus a steeper slope of the curve. This demonstrates that there is an accuracy gain from using integrators of higher orders, not only for individual trajectories but also for the full ensemble. It also demonstrates that BGSDC can deliver a particle distribution with comparable accuracy with a much larger time step than Boris. For a value of $\sigma = 1$ ns for example, Boris requires a time step of $\Delta t = 0.1$ ns whereas for BGSDC a twenty times larger step size of $\Delta t = 2$ ns suffices.

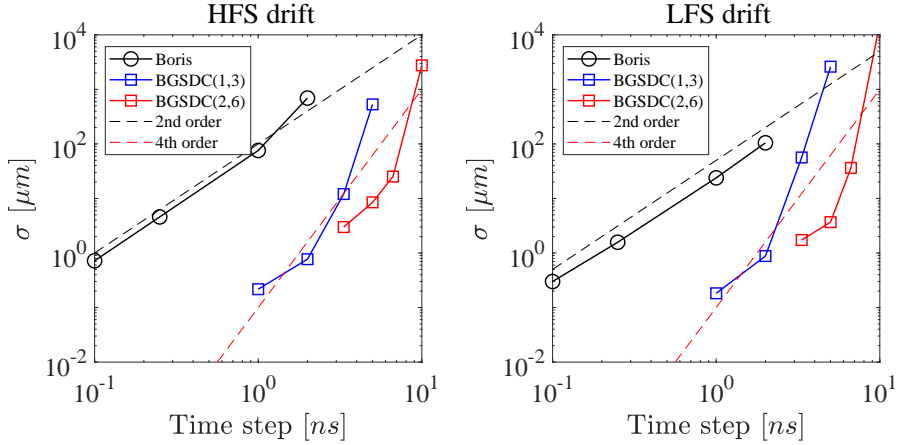


Figure 5: Standard deviation σ of drift distribution for classical Boris and BGSDC methods for different time steps in non-collisional regime in DIII-D.

Work-precision. BGSDC(2,6) with $M = 3$ Gauss-Lobatto nodes means we perform $k = 2$ iterations of GMRES-SDC on the linearised problem and $l = 6$ Picard iterations [18]. In contrast to Boris, which only needs one, BGSDC(2,6) therefore requires 19 right hand side (*RHS*) evaluations per time step. However, as shown in Fig. 2 and 3, it can provide comparable accuracy with a much larger Δt and will thus require fewer time steps. If the number of steps is sufficiently smaller to compensate for the increased work per step, BGSDC will be computationally more efficient.

To pinpoint where BGSDC starts to deliver computational gains, Fig. 6 shows the number of total RHS evaluations required by Boris to reach some standard deviation σ divided by the number of evaluations required by BGSDC(1,3). A value of $S_u > 1$ means that BGSDC(1,3) requires fewer evaluations and thus less computational work whereas $S_u < 1$ means Boris requires fewer evaluations. We assume perfect second order convergence of Boris method to interpolate between data points, which is line with the behaviour we see in Fig. 5. For the HFS, the break-even point for BGSDC is for accuracies slightly below $\sigma = 1 \mu\text{m}$ and gains increase sharply from there. A distribution with HFS $\sigma = 0.5 \mu\text{m}$ will require only about $1/1.5 \approx 66\%$ as many evaluations as when using Boris.

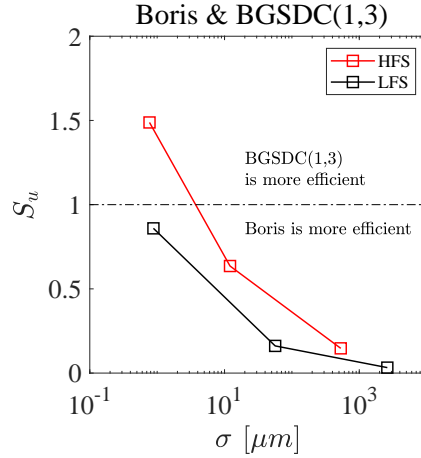


Figure 6: Ratio S_u of field evaluations required by Boris to reach some standard deviation σ divided by the number of evaluations required by BGSDC(1,3) for the DIII-D reactor.

Gains are less pronounced when looking at LFS values, where the break-even point seems to be slightly above $\sigma = 0.1 \mu m$.

3.2. Results for the DIII-D tokamak: collisional case

In the collisional case, we launch one particle 131072 times from the same position. The duration of each run is $t_{end} = 100$ ms, the same as in the collisionless case, and we use the same 2D plasma equilibrium. Fig. 7 shows 1D cross-sections of the distribution function $F(v, L, R, Z)$ against pitch angle $L = v_{\perp}/v_{\parallel}$ in a phase box for a trapped particle on the top with fixed velocity $v = 1.8 \times 10^6$ m/s, major radius $R = 2$ m, axis $Z = 0.5$ m and for a passing particle at the bottom with $v = 1.8 \times 10^6$ m/s, $R = 1.9$ m and $Z = 0.3$ m.

Boris and BGSDC both converge to the same distribution. However, BGSDC produces a stable distribution for larger time steps than Boris. For trapped orbits, the distributions provided by BGSDC with 1 ns and 10 ns time steps are very similar whereas Boris shows visible differences at a time step of 10 ns. For passing orbits, both methods require slightly smaller time steps to produce stable distributions. BGSDC has converged for a step size of 5 ns whereas Boris requires a smaller step size of 2 ns.

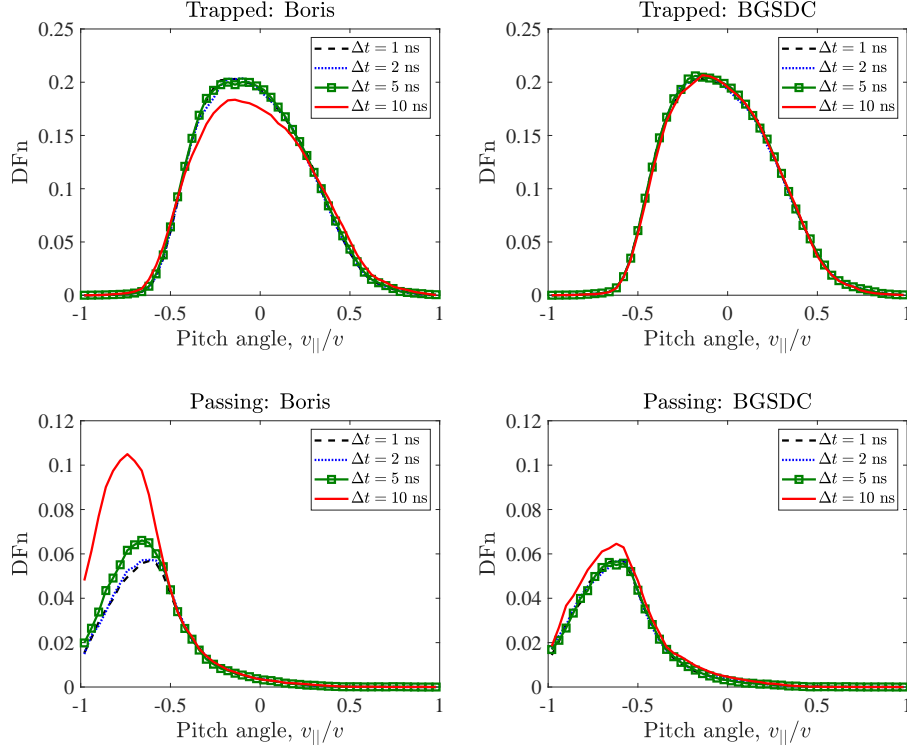


Figure 7: 1D profiles of the distribution function for DIII-D for Boris method on the left and BGSDC(2,6) on the right.

3.3. Results for the JET tokamak: non-collisional case

For JET, full orbit simulations were carried out in a 2D equilibrium for shot #92416. We use an artificial source of particles uniformly distributed in pitch angle and inside the plasma volume at a fixed injection energy. All runs last 1 s and use 65536 unique particles. As in the DIII-D runs, we do not include PFCs.

Numerical drift. Fig. 8 shows the numerical orbital drift for all particles at the end of simulation at $t_{end} = 1$ s. Results from the Boris method with time step 0.5 ns are shown on the left and from BGSDC(1,4) with 2 ns on the right. Again, the upper graphs show drift for trapped particles while the lower graphs show drift for passing particles and values for LFS are marked in black while values

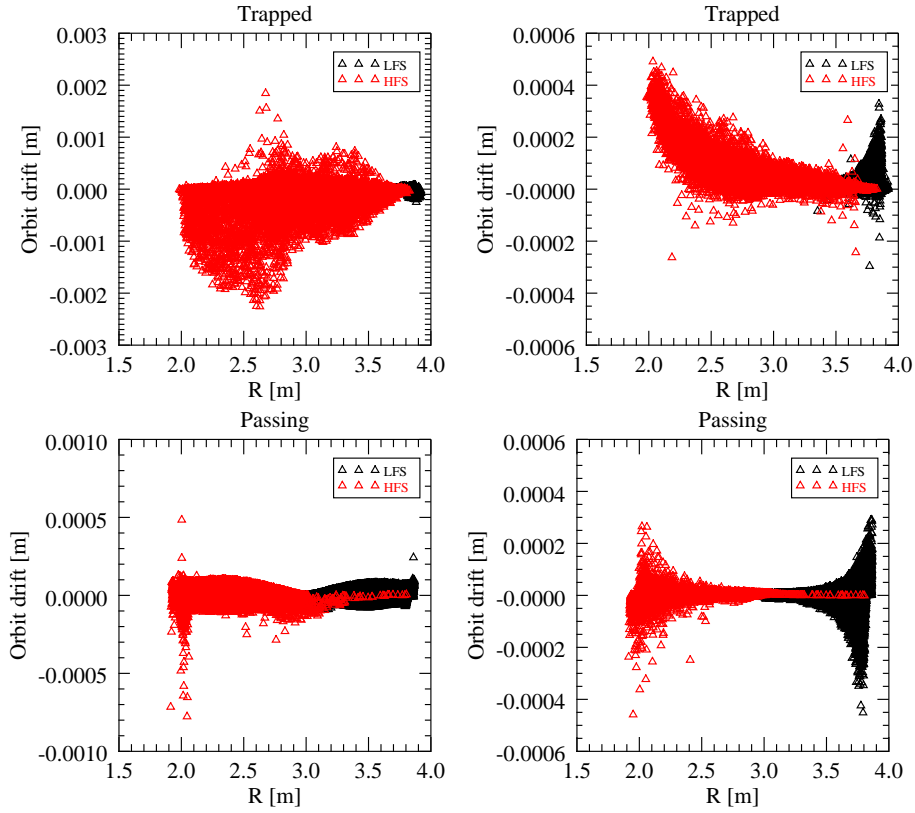


Figure 8: Particle drift for the JET tokamak after 1 s simulation time. Boris method $\Delta t = 0.5$ ns (left) and BGSDC(1,4) $\Delta t = 2$ ns (right)

for HFS are marked red. For trapped particles BGSDC(1,4) gains a maximum deviation of 5×10^{-4} m, when Boris with 4 times smaller step shows 2×10^{-3} m deviation. Please note that the y -axis scale changes. For passing particles both methods deliver comparable accuracy with BGSDC showing somewhat lower peak values.

Fig. 9 shows the resulting standard deviation σ of the drift distribution for both integrators depending on the time step. As for DIII-D, the higher order of accuracy of BGSDC leads to a steeper decrease in σ with time step size. For a fixed Δt , BGSDC produces much narrower distributions than Boris for both HFS and LFS.

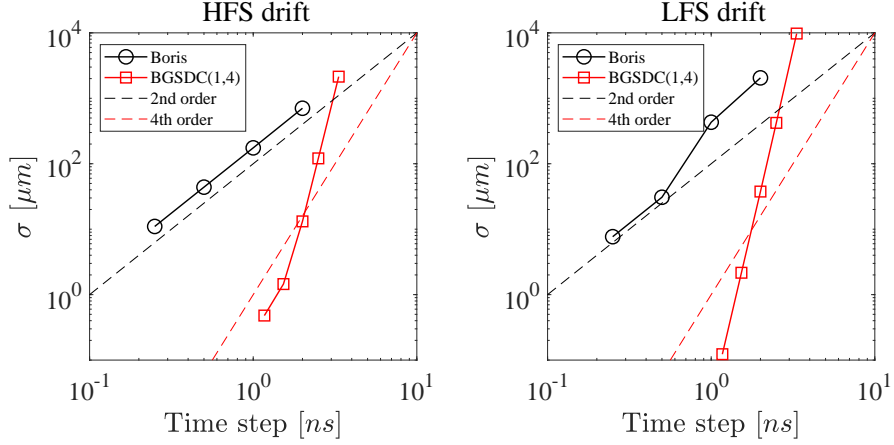


Figure 9: Standard deviation σ of drift distribution for classical Boris and BGSDC methods for different time steps in non-collisional regime in JET.

Work-precision. Fig. 10 shows again the ratio of RHS evaluations for Boris compared to BGSDC required to produce a distribution with a given σ . Results are very similar to those for DIII-D. BGSDC becomes competitive in the range between $\sigma = 0.1 \mu\text{m}$ and $\sigma = 1 \mu\text{m}$ for the HFS and LFS with better gains for HFS.

3.4. Results for the JET tokamak: collisional case

For the collisional case we launch one particle 131072 times from the same position and track it until simulated time 1 s. Fig. 11 shows 2D profiles of the distribution function in a minor cross-section of the JET tokamak. BGSDC with $\Delta t = 2$ and $\Delta t = 5$ ns as well as Boris with $\Delta t = 2$ ns deliver comparable profiles. Profiles computed with Boris with time steps 5 ns and larger show noticeable differences.

Fig. 12 and 13 show 1D profiles of the distribution function in a phase box with fixed velocity and position. In the slice shown in Fig. 12, BGSDC with $\Delta t = 2$ and $\Delta t = 5$ ns and Boris method with $\Delta t = 1$ ns produce similar profiles of $F(L)$. Small deviations can be seen on both ends for the blue line (Boris $\Delta t = 2$ ns) in the left picture and in the centre for right picture. Boris with

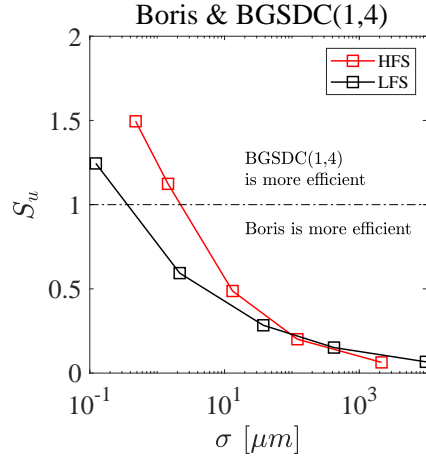


Figure 10: Ratio S_u of field evaluations required by Boris to reach some standard deviation σ divided by the number of evaluations required by BGSDC(1,4) for the JET reactor.

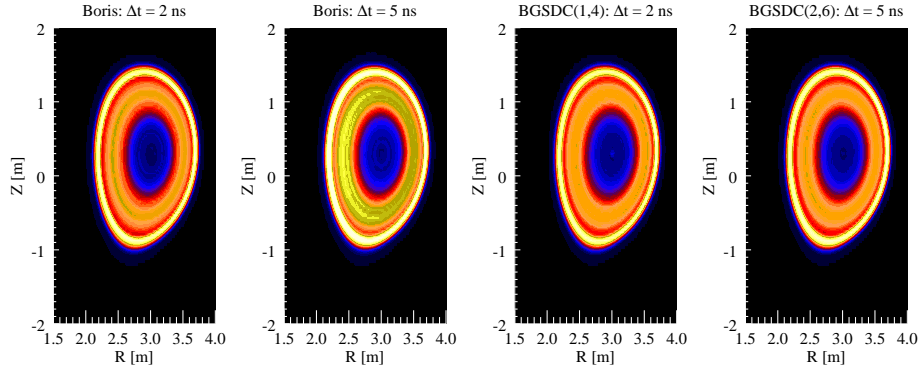


Figure 11: 2D profiles of the distribution function for fixed velocity and pitch angle.

time step ≥ 5 ns shows significant differences in the $F(L)$ profiles and the radial profiles $F(R)$ shown in Fig. 13. Similar results have been observed at different values of v, R, Z and L but are not documented here.

4. Conclusions

We compare the performance of the BGSDC time stepping algorithm against the standard Boris integrator when computing trajectories of fast ions generated

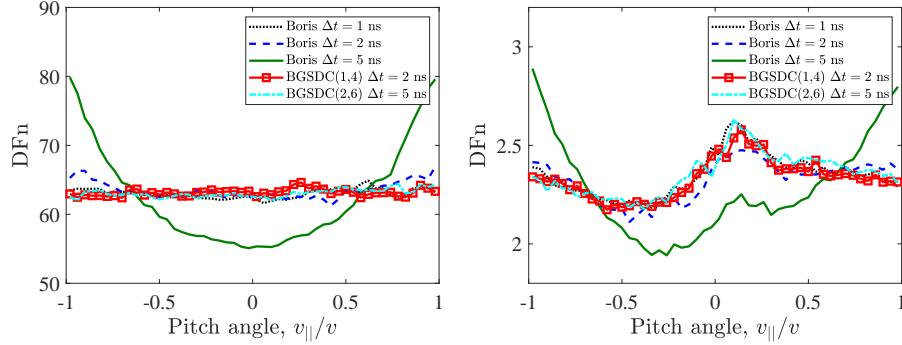


Figure 12: 1D profiles of the distribution function against pitch angle at fixed $v = 0.1 \cdot 10^6$, $R = 2.2$, $Z = -0.1$ on the left and $v = 0.5 \cdot 10^6$, $R = 2.2$, $Z = -0.5$ on the right.

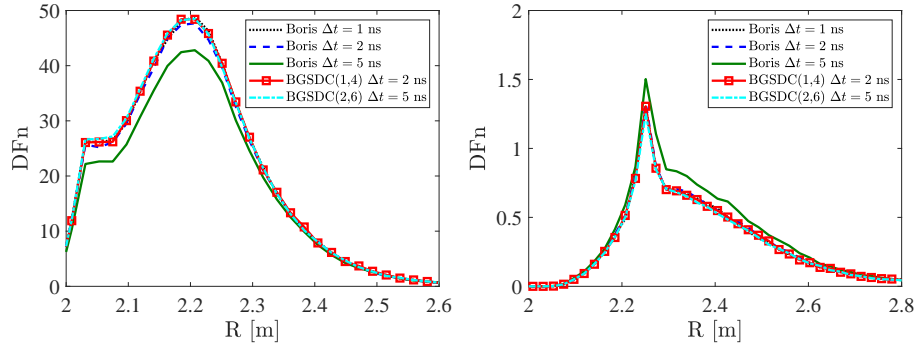


Figure 13: 1D profiles of the distribution function along major radius with $v = 0.2 \cdot 10^6$, $L = 0.2$, $Z = 0.3$ on the left and $v = 0.8 \cdot 10^6$, $L = -0.9$, $Z = 0.1$ on the right.

by neutral beam injection into a fusion reactor. Numerical examples are shown for both DIII-D and JET reactors and include non-collisional and collisional models with plasma. For the non-collisional case, the model is deterministic and we can use the standard deviation of the numerical drift distribution across all particles as a metric for solution quality. The results in this paper show that for both DIII-D and JET, BGSDC produces a substantially narrower and thus better distribution than Boris at the same time step. BGSDC can provide computational gains compared to classical Boris when trajectory simulations need to be of high precision with standard deviations of the order of $1 \mu\text{m}$ or

lower.

Detailed quantitative assessment of particle trajectories in the presence of collisions is left for future work, as there are no mathematical tools established in the fusion community to define a precise notion of accuracy in these cases. However, we show that BGSDC and Boris converge to similar distributions and that BGSDC provides stable distributions at larger time steps than Boris.

References

References

- [1] J. Artaud, et al., The CRONOS suite of codes for integrated tokamak modelling, *Nuclear Fusion* 50 (2010) 043001.
- [2] R. Hemsworth, H. Decamps, J. Graceffa, B. Schunke, M. Tanaka, M. Dremel, A. Tanga, H. D. Esch, F. Geli, J. Milnes, T. Inoue, D. Marcuzzi, P. Sonato, P. Zaccaria, Status of the ITER heating neutral beam system, *Nuclear Fusion* 49 (2009) 045006.
- [3] R. Goldston, D. McCune, H. Towner, S. Davis, R. Hawryluk, G. Schmidt, New techniques for calculating heat and particle source rates due to neutral beam injection in axisymmetric tokamaks, *Journal of Computational Physics* 43 (1981) 61 – 78.
- [4] A. Pankin, D. McCune, R. Andre, G. Bateman, A. Kritz, The tokamak monte carlo fast ion module nubeam in the national transport code collaboration library, *Computer Physics Communications* 159 (2004) 157 – 184.
- [5] K. Shinohara, Y. Suzuki, J. Kim, J. Y. Kim, Y. M. Jeon, A. Bierwage, T. Rhee, Investigation of fast ion behavior using orbit following monte-carlo code in magnetic perturbed field in KSTAR, *Nuclear Fusion* 56 (2016) 112018.

- [6] A. Snicker, S. Sipilä, T. Kurki-Suonio, Orbit-following fusion alpha wall load simulation for ITER scenario 4 including full orbit effects, *Nuclear Fusion* 52 (2012) 094011.
- [7] E. Hirvijoki, O. Asunta, T. Koskela, T. Kurki-Suonio, J. Miettunen, S. Sipilä, A. Snicker, S. Äkäslompolo, Ascot: Solving the kinetic equation of minority particle species in tokamak plasmas, *Computer Physics Communications* 185 (2014) 1310 – 1321.
- [8] R. J. Akers, E. Verwichte, T. J. Martin, S. D. Pinches, R. Lake, GPGPU Monte Carlo Calculation of Gyro-Phase Resolved Fast Ion and n-State Resolved Neutral Deuterium Distributions, in: *Proceedings of the 39th EPS Conference & 16th Int. Congress on Plasma Physics*, 2012.
- [9] J. R. Cash, A. H. Karp, A variable order runge-kutta method for initial value problems with rapidly varying right-hand sides, *ACM Trans. Math. Softw.* 16 (1990) 201–222.
- [10] G. Delzanno, E. Camporeale, On particle movers in cylindrical geometry for particle-in-cell simulations, *Journal of Computational Physics* 253 (2013) 259 – 277.
- [11] H. Qin, S. Zhang, J. Xiao, J. Liu, Y. Sun, W. M. Tang, Why is Boris algorithm so good?, *Physics of Plasmas* 20 (2013).
- [12] Y. He, Y. Sun, J. Liu, H. Qin, Volume-preserving algorithms for charged particle dynamics, *Journal of Computational Physics* 281 (2015) 135–147.
- [13] M. Quandt, C. Munz, R. Schneider, A high order relativistic particle push method for PIC simulations, in: *The 30th International Electric Propulsion Conference*, 2007, pp. 1–9. URL: <http://bibliothek.fzk.de/zb/veroeff/69220.pdf>.
- [14] M. Tao, Explicit high-order symplectic integrators for charged particles in general electromagnetic fields, *Journal of Computational Physics* 327 (2016) 245 – 251.

- [15] Y. He, Y. Sun, J. Liu, H. Qin, Higher order volume-preserving schemes for charged particle dynamics, *Journal of Computational Physics* 305 (2016) 172–184.
- [16] E. Hairer, C. Lubich, Symmetric multistep methods for charged-particle dynamics, *Journal of Computational Mathematics* 3 (2017) 205–218.
- [17] T. Umeda, A three-step boris integrator for lorentz force equation of charged particles, *Computer Physics Communications* 228 (2018) 1 – 4.
- [18] K. Tretiak, D. Ruprecht, An arbitrary order time-stepping algorithm for tracking particles in inhomogeneous magnetic fields, *Journal of Computational Physics: X* 4 (2019) 100036.
- [19] O. Asunta, J. Govenius, R. Budny, M. Gorelenkova, G. Tardini, T. Kurki-Suonio, A. Salmi, S. Sipilä, Modelling neutral beams in fusion devices: Beamlet-based model for fast particle simulations, *Computer Physics Communications* 188 (2015) 33 – 46.
- [20] R. Akers, K. Tretiak, BGSDC particle tracker, 2018. URL: https://git.iter.org/projects/TRAJ/repos/locust/browse?at=BGSDC_integrator.
- [21] F. Imbeaux, S. Pinches, J. Lister, Y. Buravand, T. Casper, B. Duval, B. Guillerminet, M. Hosokawa, W. Houlberg, P. Huynh, S. Kim, G. Manduchi, M. Owsiak, B. Palak, M. Plociennik, G. Rouault, O. Sauter, P. Strand, Design and first applications of the ITER integrated modelling & analysis suite, *Nuclear Fusion* 55 (2015) 123006.
- [22] M. Winkel, R. Speck, D. Ruprecht, A high-order Boris integrator, *Journal of Computational Physics* 295 (2015) 456–474.
- [23] J. P. Boris, Relativistic plasma simulation-optimization of a hybrid code, in: *Proceedings of the Fourth Conference on Numerical Simulation of Plasmas*, Naval Research Laboratory, Washington, DC, 1970, pp. 3–67.

- [24] A. Dutt, L. Greengard, V. Rokhlin, Spectral deferred correction methods for ordinary differential equations, *BIT Numerical Mathematics* 40 (2000) 241–266.
- [25] J. Huang, J. Jia, M. Minion, Accelerating the convergence of spectral deferred correction methods, *Journal of Computational Physics* 214 (2006) 633 – 656.
- [26] C. K. Birdsall, A. B. Langdon, *Plasma physics via computer simulation*, McGraw-Hill, New York, 1985.
- [27] E. Hairer, S. P. Nørsett, G. Wanner, *Solving Ordinary Differential Equations I: Nonstiff problems*, 2nd ed., Springer-Verlag Berlin Heidelberg, 1993. URL: <http://dx.doi.org/10.1007/978-3-540-78862-1>.
- [28] E. Hairer, C. Lubich, G. Wanner, *Geometric numerical integration: structure-preserving algorithms for ordinary differential equations*, Springer Verlag Berlin Heidelberg New York, 2002. URL: <http://dx.doi.org/10.1007/3-540-30666-8>.
- [29] E. Hairer, G. Wanner, *Solving Ordinary Differential Equations II: Stiff problems*, Springer-Verlag Berlin Heidelberg, 1996. URL: <http://dx.doi.org/10.1007/978-3-642-05221-7>.
- [30] M. L. Minion, Semi-implicit spectral deferred correction methods for ordinary differential equations, *Communications in Mathematical Sciences* 1 (2003) 471–500.
- [31] C. T. Kelley, *Iterative Methods for Linear and Nonlinear Equations*, Society for Industrial and Applied Mathematics, 1995. URL: <http://dx.doi.org/10.1137/1.9781611970944>.
- [32] R. Akers, et al., High fidelity simulations of fast ion power flux driven by 3D field perturbations on ITER, Available at <https://nucleus.iaea.org/sites/fusionportal/SharedDocuments/FEC2016/fec2016-preprints/preprint0489.pdf>, (2016).

- [33] J. Milnes, N. B. Aye, F. Dhalla, G. Fishpool, J. Hill, I. Katramados, R. Martin, G. Naylor, T. O’Gorman, R. Scannell, the MAST Upgrade team, Mast upgrade - construction status, 2015. URL: <https://arxiv.org/abs/1503.06677>.
- [34] M. Fitzgerald, J. Buchanan, R. Akers, B. Breizma, S. Sharapov, HALO: A full-orbit model of nonlinear interaction of fast particles with eigenmodes, 2018. URL: http://www.euro-fusionscipub.org/wp-content/uploads/eurofusion/WP17ERPR18_21459_submitted.pdf.
- [35] M. Van Zeeland, N. Ferraro, B. Grierson, W. Heidbrink, G. Kramer, C. Lasnier, D. Pace, S. Allen, X. Chen, T. Evans, M. García-Muñoz, J. Hanson, M. Lanctot, L. Lao, W. Meyer, R. Moyer, R. Nazikian, D. Orlov, C. Paz-Soldan, A. Wingen, Fast ion transport during applied 3D magnetic perturbations on DIII-D, Nuclear Fusion 55 (2015) 073028.